Journal of King Saud University - Science 36 (2024) 103271

Contents lists available at ScienceDirect

Journal of King Saud University - Science

journal homepage: www.sciencedirect.com

Full Length Article

Influence of dipole interaction on the quantum correlation detection and teleportation in a qubit-field system

Hanaa Abu-Zinadah [a], E.M. Khalil [b,c,*]

[a] Department of Mathematics and Statistics, College of Science, University of Jeddah, Jeddah, Saudi Arabia
[b] Department of Mathematics, College of Science, Taif University, P.O. Box 11099, Taif 21944, Saudi Arabia
[c] Mathematics Department, Faculty of Science, Al-Azhar University, Nasr City 11884, Cairo, Egypt

ARTICLE INFO

Keywords:
Dipole interaction
Teleportation
Steering
Entanglement
Non-locality

ABSTRACT

This study examines the analysis of the teleportation process in a two-qubit state, particularly scrutinizing the interplay of atomic dipole coupling interaction, the detuning parameter, photon count, and the surrounding environment. Our investigation assumes the existence of a teleportation channel comprising two-qubit systems interacting with a photon field enveloped by the dephasing environment. Within this framework, we closely examine the quantum correlations exhibited by the teleported state, encompassing dimensions of entanglement, steering, and non-locality. Our results underscore the pivotal role played by the initial state of the atomic and field subsystems in shaping quantum relations. The dipole coupling has a profound impact, significantly enhancing the three quantifiers. Particularly, the entanglement changes from a de-entangled state to a partially entangled state. On the other hand, the detuning parameter introduces distortion in the quantum correlations, a phenomenon that can be effectively mitigated by controlling the dipole coupling.

1. Introduction

Realistic experiments demonstrate that open quantum systems inevitably exchange energy with their surrounding environment during interactions. This energy exchange gradually erodes the system's quantum properties, even at specific instances, potentially hindering their exploitation for practical applications (Yu and Eberly, 2009; Almeida et al., 2007). The detrimental effects of decoherence are particularly pronounced in the context of independent qubits, each embedded in its environment, which is essential for implementing quantum communication and information protocols with distant, individually addressable particles (Ladd et al., 2010; Abd-Rabboul et al., 2021). In response to the detrimental effects of decoherence on quantum correlations, researchers are exploring the possibility of designing effective and feasible quantum models that can safeguard these delicate correlations from the harmful influence of noise (Gisin and Thew, 2007). Conversely, significant attention has been devoted to Markovian designs, which involve crafting appropriate quantum systems capable of preserving quantum memory effects (Man et al., 2018). The non-Markovian systems exhibit fundamental characteristics that are essential for reviving quantum entanglement, regardless of whether they possess a bosonic or fermionic quantum nature (Fanchini et al., 2010; Rahman et al., 2023) or a classical nature (e.g., random noise, random field, noisy phase laser) (Abd-Rabbou et al., 2023c). In quantum systems, the presence of a thermal environment, characterized by its temperature, poses a significant challenge as it can induce decoherence, ultimately leading to the degradation of quantum correlations (Bellomo et al., 2008; Yan and Yue, 2013). This phenomenon has garnered considerable attention in recent research efforts, particularly in understanding its impact on entanglement dynamics. Moreover, the entanglement of multi-qubit quantum systems under the influence of both thermal and dephasing environments has been a subject of investigation (Hu et al., 2009; Hu, 2012). Additionally, quantum systems are often subjected to various noisy channels, such as amplitude damping, depolarizing, and phase damping channels, which disrupt quantum correlations, leading to information loss and diminished entanglement (Abd-Rabbou et al., 2019, 2023a). Therefore, this paper aims to explore the effects of the thermal environment and common dephasing environment on entanglement dynamics, particularly in the presence of n-sequential $\sin^2$-pulse shapes (Abd-Rabbou et al., 2023b).

Quantum information theory was adopted to study the entanglement of quantum systems because of its key role in knowing the main characteristics in the interaction process between parts of the system, such as quantum encryption (Bouwmeester et al., 2013), quantum computations, geometric quantum computation (Wang, 2009; Guo et al., 2019), and dense cryptography (Hiroshima, 2001). Quantum

* Corresponding author at: Department of Mathematics, College of Science, Taif University, P.O. Box 11099, Taif 21944, Saudi Arabia.
E-mail addresses: Hhabuznadah@uj.edu.sa (H. Abu-Zinadah), eiedkhalil@tu.edu.sa (E.M. Khalil).

https://doi.org/10.1016/j.jksus.2024.103271
Received 27 November 2023; Received in revised form 5 May 2024; Accepted 22 May 2024
Available online 27 May 2024

correlations underpin the fundamental principles of quantum information processing. These correlations, including entanglement, nonlocality, steering, and discord, arise from interactions between parts of complex quantum systems (Abd-Rabbou et al., 2022; Youssef et al., 2023). Attention has been paid to studying the features of quantum correlations in encryption and teleportation on a large scale, both theoretically and experimentally (Mirmasoudi and Ahadpour, 2018). Using the previous quantum entanglement in which the sender and receiver participated, quantum teleportation and dense cryptography were implemented (Omri et al., 2022; Abd-Rabbou and Khalil, 2022). Therefore, many different quantum models have been designed to generate quantum correlation theoretically and experimentally. For example, a surface polariton-supporting method has been proposed to generate dually entangled electrons (Asban and García de Abajo, 2021). A shared phonon tank was designed to form non-classical correlations between two excited qubits (Krzywda and Roszak, 2016). The entanglement and discord periods generated from an unbound system when exposed to a combined thermal or pressurized tank are investigated in Gallego et al. (2012). A laboratory-viable scheme for generating a multi-mode quantum light source using a non-degenerate four-wave mixing procedure in a thermally controlled atomic vapor cell was designed in Cao et al. (2017). In addition, another practical scheme has been proposed, therefore, to generate quantum correlations and experimentally control the parameters of the quantum system to study entanglement periods (Ding et al., 2012).

The central aim of this study is to explore the viability of teleporting a pair of quantum qubits through an atom-field interaction within a dephasing environment. Teleported qubits undergo instantaneous exposure to various effects originating from the teleportation channel, encompassing factors such as the channel's initial state, photon count, detuning, dipole coupling, and the decay rate of the dephasing environment. These factors can exert either augmenting or diminishing influences on the teleported quantum correlations. Prior research has indicated that dipole coupling has the potential to enhance quantum correlations (Khalil and Abd-Rabbou, 2022; Abd-Rabbou and Khalil, 2022). Our objective is to ascertain whether this enhancement extends to teleported quantum correlations and whether it can ameliorate the adverse effects of the dephasing environment and detuning. To address these inquiries, we will scrutinize the entanglement, steering, and nonlocality of the teleported state. This paper is structured as follows: Section 2 introduces the Hamiltonian model of the quantum channel and its density operator, incorporating the effects of the dephasing environment. Sections 3 and 4 provide a concise overview of the teleportation process and quantum correlation quantifiers, including entanglement, steering, and nonlocality. Section 5 presents our results, exploring the impact of teleportation channel parameters on quantum correlations. Finally, Section 6 summarizes our findings and concludes the paper.

2. Physical model of channel

Consider two partners, referred to as Jon in lab (a) and Rob in lab (b), who share a quantum channel comprising a two-qubit system with a frequency ω_q. These qubits are coupled to each other through the coupling parameter, λ_1, and simultaneously interact with a single mode of an ideal bosonic cavity with a frequency denoted as ω_c. The system is described in Fig. 1. Mathematically, the Hamiltonian model of the quantum channel, under the rotating wave approximation, can be expressed as follows (Abd-Rabbou et al., 2024)

$$\frac{\hat{H}}{\hbar} = \omega_c \hat{\Psi}^\dagger \hat{\Psi} + \frac{\omega_q}{2} \sum_{i=a,b} \hat{\sigma}_z^{(i)} + \lambda_1 (\hat{\sigma}_+^{(a)} \hat{\sigma}_-^{(b)} + \hat{\sigma}_-^{(a)} \hat{\sigma}_+^{(b)}) + \lambda_2 \sum_{i=a,b} \left(\hat{\Psi} \hat{\sigma}_+^{(i)} + \hat{\Psi}^\dagger \hat{\sigma}_-^{(i)} \right), \tag{1}$$

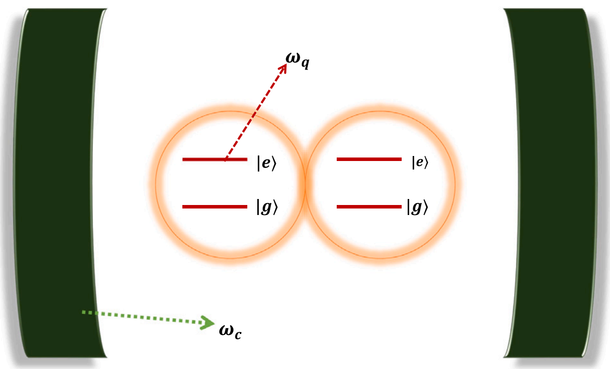

Fig. 1. A Sketch of a two-qubit system located inside a cavity field. Here, ω_c, and ω_q are the frequencies of the quantized cavity field, and the two-qubit system.

where $\hat{\Psi}$ ($\hat{\Psi}^\dagger$) is the creation (annihilation) operator of the cavity, $\hat{\sigma}_z^{(i)}$ and $\hat{\sigma}_\pm^{(i)}$ are the z-Pauli operator and ladder operator of the two-qubit, respectively. λ_2 is the field-qubit coupling exchange.

Now, we direct our focus toward determining the dynamic operators governing the current system. To achieve this, the application of well-established principles, such as the Heisenberg equations of motion, becomes imperative

$$\frac{d\hat{A}}{dt} = -\frac{i}{\hbar}[\hat{A}, \hat{H}] + \frac{\partial \hat{A}}{\partial t}, \tag{2}$$

where $\hat{A}$ is any arbitrary operator. Through meticulous calculations for the operators $\hat{\Psi}^\dagger\hat{\Psi}$ and $\hat{\sigma}_z^{(i)}$, we can obtain the following set of the interrelated equations of motion ($\hbar$=1)

$$\begin{aligned} \frac{d\hat{\Psi}^\dagger\hat{\Psi}}{dt} &= \sum_{i=a,b} \lambda_2 (\hat{\Psi}^\dagger \hat{\sigma}_-^{(i)} + \hat{\Psi} \hat{\sigma}_+^{(i)}), \\ \frac{d\hat{\sigma}_z^{(i)}}{dt} &= -2 \sum_{i=a,b} \lambda_2 (\hat{\Psi}^\dagger \sigma_-^{(i)} + \hat{\Psi} \sigma_+^{(i)}). \end{aligned} \tag{3}$$

From these previous equations, one can get the constants of the motion of the channel model as

$$\hat{H}_0 = \hat{\Psi}^\dagger\hat{\Psi} + \frac{1}{2}\sum_{i=a,b} \hat{\sigma}_z^{(i)}, \tag{4}$$

$$\hat{H}_{eff} = \frac{\Delta}{2}\sum_{i=a,b} \hat{\sigma}_z^{(i)} + \lambda_1 (\hat{\sigma}_+^{(a)} \hat{\sigma}_-^{(b)} + \hat{\sigma}_-^{(a)} \hat{\sigma}_+^{(b)}) + \lambda_2 \sum_{i=a,b} \left(\hat{\Psi} \hat{\sigma}_+^{(i)} + \hat{\Psi}^\dagger \hat{\sigma}_-^{(i)} \right), \tag{5}$$

where $\Delta = \omega_q - 2\omega_c$, and $[\hat{H}_0, \hat{H}_{eff}] = 0$. In what follows we shall obtain the dynamical density operator $\hat{\rho}_{ab}(t)$ of the effective Hamiltonian $\hat{H}_{eff}$ in Eq. (5).

To get $\hat{\rho}_{ab}(t)$ of the channel between Jon and Rob, we can employ the master equation, which is expressed as (Manzano, 2020)

$$\frac{d\rho(t)}{dt} = -i\left[\hat{H}, \rho(t)\right] + \mathscr{L}\rho(t), \tag{6}$$

where

$$\mathscr{L}\rho(t) = \frac{\gamma}{2}\sum_i \left(\sigma_z^{(i)}\rho(t)\sigma_z^{(i)} - \rho(t) \right), \tag{7}$$

here γ signifies the decay rate linked to the environmental interactions. Our specific scenario operates under the assumption that the channel is not entirely isolated from its surroundings, a condition that often aligns with a more realistic representation of the physical system. It assumed that the two-qubit system is simultaneously coupled to a global dephasing reservoir. Nevertheless, it is essential to note that when $\gamma = 0$, a special scenario emerges in which the channel remains entirely devoid of interactions with its environment.

According to Eqs. (5) and (6), we can get the following system of ordinary differential equations (ODE)

$$\begin{aligned}
&\rho'_{1,1}(t) = i\nu_1\left(\rho_{1,2}(t)+\rho_{1,3}(t)-\rho_{2,1}(t)-\rho_{3,1}(t)\right),\\
&\rho'_{2,2}(t) = i\left(\lambda_1\left(\rho_{2,3}(t)-\rho_{3,2}(t)\right)+\nu_1\left(\rho_{2,1}(t)-\rho_{1,2}(t)\right)+\nu_2\left(\rho_{2,4}(t)-\rho_{4,2}(t)\right)\right),\\
&\rho'_{3,3}(t) = i\left(\lambda_1\left(\rho_{3,2}(t)-\rho_{2,3}(t)\right)+\nu_1\left(\rho_{3,1}(t)-\rho_{1,3}(t)\right)+\nu_2\left(\rho_{3,4}(t)-\rho_{4,3}(t)\right)\right),\\
&\rho'_{4,4}(t) = -i\nu_2\left(\rho_{2,4}(t)+\rho_{3,4}(t)-\rho_{4,2}(t)-\rho_{4,3}(t)\right),\\
&\rho'_{1,2}(t) = \beta\rho_{1,2}(t)+i\left(\lambda_1\rho_{1,3}(t)+\nu_2\rho_{1,4}(t)\right)+i\nu_1\left(\rho_{1,1}(t)-\rho_{2,2}(t)-\rho_{3,2}(t)\right)\\
&= (\rho'_{2,1}(t))^*,\\
&\rho'_{1,3}(t) = \beta\rho_{1,3}(t)+i\lambda_1\rho_{1,2}(t)+i\nu_2\rho_{1,4}(t)+i\nu_1\left(\rho_{1,1}(t)-\rho_{2,3}(t)-\rho_{3,3}(t)\right)\\
&= (\rho'_{3,1}(t))^*,\\
&\rho'_{1,4}(t) = 2\beta\rho_{1,4}(t)+i\nu_2\left(\rho_{1,2}(t)+\rho_{1,3}(t)\right)-i\nu_1\left(\rho_{2,4}(t)+\rho_{3,4}(t)\right) = (\rho'_{4,1}(t))^*,\\
&\rho'_{2,3}(t) = -2\gamma\rho_{2,3}(t)+i\lambda_1\left(\rho_{2,2}(t)-\rho_{3,3}(t)\right)+i\nu_2\left(\rho_{2,4}(t)-\rho_{4,3}(t)\right)\\
&-i\nu_1\left(\rho_{1,3}(t)-\rho_{2,1}(t)\right) = (\rho'_{3,2}(t))^*,\\
&\rho'_{2,4}(t) = \beta\rho_{2,4}(t)-i\lambda_1\rho_{3,4}(t)-i\nu_1\rho_{1,4}(t)+i\nu_2\left(\rho_{2,2}(t)+\rho_{2,3}(t)-\rho_{4,4}(t)\right)\\
&= (\rho'_{4,2}(t))^*,\\
&\rho'_{3,4}(t) = \beta\rho_{3,4}(t)-i\lambda_1\rho_{2,4}(t)-i\nu_1\rho_{1,4}(t)+i\nu_2\left(\rho_{3,2}(t)+\rho_{3,3}(t)-\rho_{4,4}(t)\right)\\
&= (\rho'_{4,3}(t))^*,
\end{aligned} \tag{8}$$

where $\nu_1 = \lambda_2\sqrt{n+1}$, $\nu_2 = \lambda_2\sqrt{n+2}$, and $\beta = -\gamma - i\frac{\Delta}{2}$. Via solving the linear ODE, one can find the density operator $\hat{\rho}_{ab}(t)$ of the system as

$$\hat{\rho}_{ab}(t) = \hat{\rho}_{ab}(0).e^{\hat{\mathscr{E}}t}, \tag{9}$$

here $\hat{\mathscr{E}}$ is the coefficients matrix of the ODE (8). However, $\hat{\rho}_{ab}(0)$ is the initial state of the system, it is given by

$$\hat{\rho}_{ab}(0) = \mu|\Phi^+\rangle\langle\Phi^+| + (1-\mu)|\Psi^+\rangle\langle\Psi^+|. \tag{10}$$

where, $|\Phi^+\rangle = \frac{|ee\rangle+|gg\rangle}{\sqrt{2}}$, $|\Psi^+\rangle = \frac{|eg\rangle+|ge\rangle}{\sqrt{2}}$. Moreover, μ is the setting state of initial system, at $\mu = 0$ or 1, $\hat{\rho}_{ab}(0)$ is maximally entangled state, and a separable state at $\mu = 0.5$.

3. Teleportation process

The phenomenon of teleporting an entangled state between two distinct labs through a quantum channel has been introduced in the work of Lee and Kim (2000). Our methodology involves the utilization of the decayed density operator ρ_{ab} as a communication channel, for transferring the state $|\psi\rangle_{in} = \cos\theta/2|00\rangle + \sin\theta/2|11\rangle$ between two key participants: Jon and Rob. In this collaborative effort, they both share the state (9) as their communication conduit, and the output state can be obtained by (Abd-Rabboul et al., 2021)

$$\hat{\rho}_{out} = \sum_{n,m=0}^{3} Tr(\hat{\mathscr{B}}_n\hat{\rho}_{ab})Tr(\hat{\mathscr{B}}_m\hat{\rho}_{ab})(\hat{\sigma}_n\otimes\hat{\sigma}_m).|\psi\rangle_{in\cdot in}\langle\psi|.(\hat{\sigma}_n\otimes\hat{\sigma}_m), \tag{11}$$

where

$$\begin{aligned}
&\hat{\mathscr{B}}_{1,2} = |\Phi^\mp\rangle\langle\Phi^\mp|, \qquad \hat{\mathscr{B}}_{0,3} = |\Psi^\mp\rangle\langle\Psi^\mp|,\\
&|\Psi^\pm\rangle = \frac{|eg\rangle \pm |ge\rangle}{\sqrt{2}}, \qquad |\Phi^\pm\rangle = \frac{|ee\rangle \pm |gg\rangle}{\sqrt{2}}.
\end{aligned} \tag{12}$$

After performing a series of algebraic computations using eqs (9–12), we have derived the subsequent equation representing the teleported state of the final output as

$$\hat{\rho}_{out} = \begin{pmatrix} \varrho_{11} & 0 & 0 & \varrho_{14} \\ 0 & \varrho_{22} & \varrho_{23} & 0 \\ 0 & \varrho_{32} & \varrho_{33} & 0 \\ \varrho_{41} & 0 & 0 & \varrho_{44} \end{pmatrix}; \tag{13}$$

where,

$$\begin{aligned}
&\varrho_{11} = \sin^2\left(\frac{\theta}{2}\right)\left(\rho_{1,1}(t)+\rho_{4,4}(t)\right)^2 + \cos^2\left(\frac{\theta}{2}\right)\left(\rho_{2,2}(t)+\rho_{3,3}(t)\right)^2\\
&\varrho_{22} = \left(\rho_{2,2}(t)+\rho_{3,3}(t)\right)\left(\rho_{1,1}(t)+\rho_{4,4}(t)\right) = \varrho_{33},\\
&\varrho_{44} = \sin^2\left(\frac{\theta}{2}\right)\left(\rho_{2,2}(t)+\rho_{3,3}(t)\right)^2 + \cos^2\left(\frac{\theta}{2}\right)\left(\rho_{1,1}(t)+\rho_{4,4}(t)\right)^2,\\
&\varrho_{14} = \frac{1}{2}\sin(\theta)\left(\left(\rho_{2,3}(t)+\rho_{3,2}(t)\right)^2 + \left(\rho_{1,4}(t)+\rho_{4,1}(t)\right)^2\right) = \varrho_{41}\\
&\varrho_{23} = \sin(\theta)\left(\rho_{2,3}(t)+\rho_{3,2}(t)\right)\left(\rho_{1,4}(t)+\rho_{4,1}(t)\right) = \varrho_{32};
\end{aligned} \tag{14}$$

Hereinafter, we employ the concurrence, 3-steering, and Bell non-locality to examine the quantum correlation of the teleported state.

4. Quantum correlation measure

The fundamental concepts of quantum entanglement, steering, and non-locality are presented in this section as potent expressions of quantum correlations. States demonstrating entanglement and steerability can be quantified via metrics like concurrence and 3-steering, respectively. Notably, states that transgress Bell inequalities exemplify the most formidable correlations, signifying inherent non-locality between qubits when subjected to optimal measurement procedures.

4.1. Entanglement by concurrence

The degree of entanglement existing between two qubits can be effectively quantified through a well-established metric known as concurrence (Coffman et al., 2000). Concurrence serves as a reliable indicator of the entanglement strength within the quantum system, offering valuable insights into the interconnection between qubits. This quantification enables a more precise assessment of the quantum correlations and their potential impact on the system's overall behavior. The quantification of entanglement, whether in pure or mixed quantum states, is conducted through the evaluation of eigenvalues (Λ_i) of the matrix $\rho_{ab}\tilde{\rho}_{ab}$. Here, $\tilde{\rho}_{ab} == \hat{\sigma}_y \otimes \hat{\sigma}_y.\hat{\rho}^*_{ab}.\hat{\sigma}_y \otimes \hat{\sigma}_y$ which is derived from the hermitian conjugate of original density operator $\hat{\rho}^*_{ab}$ and through the tensor product with Pauli spin matrices, $\hat{\sigma}_y\otimes\hat{\sigma}_y$. The concurrence metric is formally defined as follows

$$\mathscr{C}(\hat{\rho}_{ab}) = \max\left\{0, \sqrt{\Lambda_1} - \sqrt{\Lambda_2} - \sqrt{\Lambda_3} - \sqrt{\Lambda_4}\right\}, \tag{15}$$

where $\Lambda_1 \geq \Lambda_2 \geq \Lambda_3 \geq \Lambda_4 \geq 0$.

4.2. Steering

In quantum information theory, 3-steering represents a concept that delves into the phenomenon of steering, which is a manifestation of quantum correlations. Steering involves the possibility of one quantum system indirectly influencing the state of another. In terms of three observable measurements on the two qubits (a) and (b), say $\hat{\alpha}^a_i.\hat{\sigma}^a_i$ and $\hat{\alpha}^b_i.\hat{\sigma}^b_i$, the steering inequality can be expressed by (Costa and Angelo, 2016)

$$\mathscr{S}_3(\hat{\rho}_{ab}, \hat{\alpha}) = \frac{1}{\sqrt{3}}\left|\sum_{i=1}^{3} Tr(\rho_{ab}\hat{\alpha}^a_i.\hat{\sigma}^a_i \otimes \hat{\alpha}^b_i.\hat{\sigma}^b_i)\right| \leq 1, \tag{16}$$

where $\hat{\alpha}^{a,b}_i \in \mathbb{R}^3$ represent a set of measurement directions. Using the Pauli spin matrices of two-qubit as measurements, and considering the quantum state is maximally violated inequality (16), then we can write the amount of steering as

$$\mathscr{S}_3(\hat{\rho}_{ab}) = \sqrt{\sum_{i=1}^{3} m_i^2(\hat{\rho}_{ab})}. \tag{17}$$

here $m_i(\hat{\rho}_{ab})$ are the eigenvalues of the matrix $\sqrt{M^\dagger(\hat{\rho}_{ab})M(\hat{\rho}_{ab})}$, where $M(\hat{\rho}_{ab}) = Tr[\hat{\rho}_{ab}\hat{\sigma}_i \otimes \hat{\sigma}_j]$. In the normalization form, the possibility of a

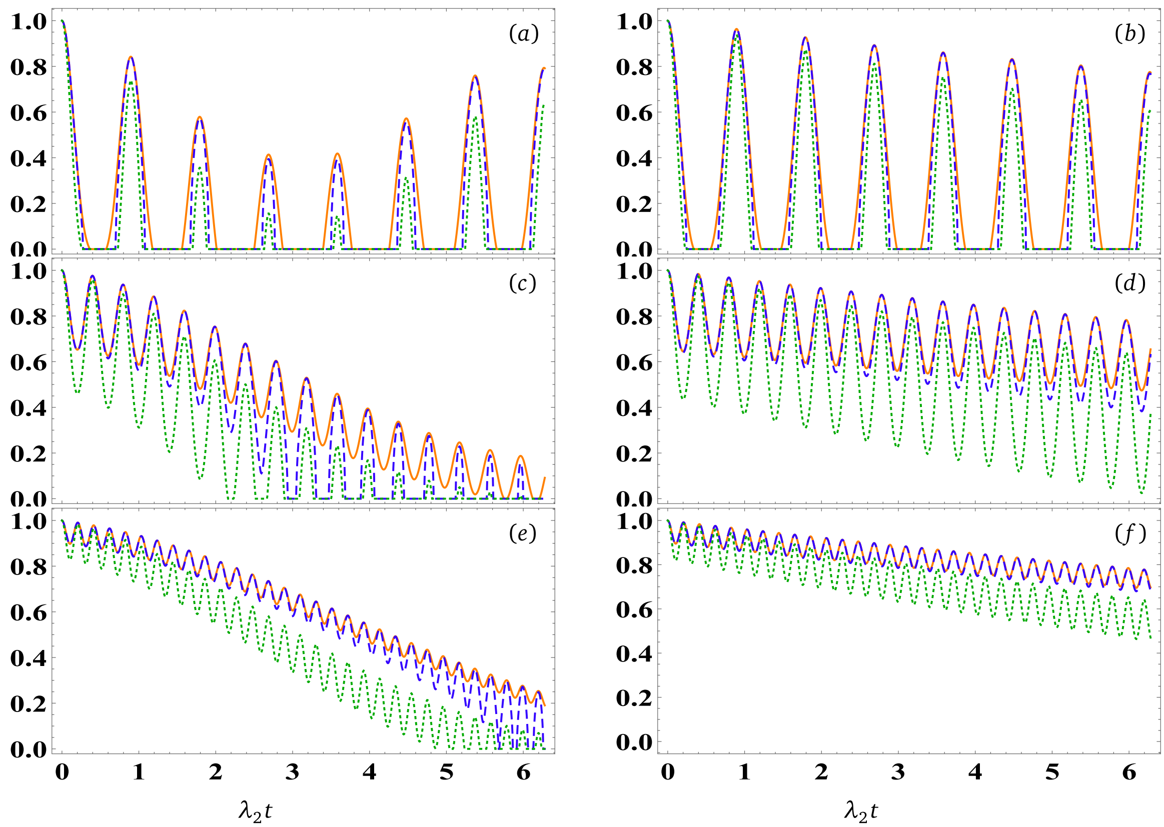

Fig. 2. The temporal evolution of quantum correlations $\mathscr{C}$ (solid-orange-curve), $\mathscr{S}_3$ (dashed-blue-curve), and $\mathbb{B}_n$ (dotted-green-curve) against the scaled time $\lambda_2 t$, where $\theta = \pi/2$, $n = 0$, $\gamma = 0.01$ and $\Delta = 0.1$. In the Left panels: $\mu = 1$, (a) $\lambda_1 = 5$, (c) $\lambda_1 = 15$, (e) $\lambda_1 = 30$. In the right panels: (b, d, f) are the same as (a, c, e), but $\mu = 0$.

qubit (a) steerer (b) can be redefined as (Fan et al., 2021)

$$\mathscr{S}(\hat{\rho}_{ab}) = \sqrt{\frac{\max\{0, \mathscr{S}_3^2(\hat{\rho}_{ab}) - 1\}}{2}}, \tag{18}$$

where $\mathscr{S}(\hat{\rho}_{ab}) \in [0, 1]$. In this formula, one can compare between the general behavior of steering and entanglement.

4.3. Bell non-locality

For deep investigation, we shall use the Bell non-locality, which is a phenomenon wherein entangled states correlations that cannot be elucidated by any local hidden variable theory (Clauser et al., 1970). This concept provides us with profound insights into the intricate nature of quantum correlations. In the case of a two-qubit state with X-shaped, the Bell non-locality is given by

$$\mathbb{B}(\hat{\rho}_{ab}) = 2\max[\mathbb{B}_1, \mathbb{B}_2], \qquad \mathbb{B}_1 = \sqrt{m_1^2 + m_2^2}, \text{ and } \qquad \mathbb{B}_2 = \sqrt{m_1^2 + m_3^2}, \tag{19}$$

where, m_i are the three eigenvalues of the matrix $\sqrt{M^{\dagger}(\hat{\rho}_{ab})M(\hat{\rho}_{ab})}$, and $M(\hat{\rho}_{ab}) = Tr[\hat{\rho}_{ab}\hat{\sigma}_i \otimes \hat{\sigma}_j]$. In the normalization form the Bell function is given by (Mohammed et al., 2023)

$$\mathbb{B}_N(\hat{\rho}_{ab}) = \max\left[0, \frac{\mathbb{B}(\hat{\rho}_{ab}) - 2}{\mathbb{B}_{max} - 2}\right], \tag{20}$$

where $B_{max} = 2\sqrt{2}$.

5. Results and discussion

Fig. 2 provides a comprehensive visualization of the quantum correlations characterizing the teleported state through a damped atomic-field channel. In this study, we consider two distinct initial scenarios for the channel, one with $\mu = 0$ and the other with $\mu = 1$, while the channel parameters are set at $\Delta = 0.1$ and $\gamma = 0.01$, with the field initially in the vacuum state ($n = 0$). By varying the dipole coupling (e.g. $\lambda_1 = 5, 15$ and 30), the discernible hierarchy among quantum correlations emerges, with the general order being maximum entanglement ≥ steering ≥ non-locality. This hierarchy illustrates the interplay of quantum correlations and underscores that the teleported information through the channel adheres to a distinct hierarchy of quantum correlations. In the first scenario, represented by $\mu = 1$ (as depicted in the left panels), and with variations in the coupling parameter λ_1. All three quantifiers commence from their respective maximum values, which are one. Fig. 2(a) shows that these three correlations exhibit oscillatory behavior characterized by periods of sudden decline and resurgence, each subsequent phase displaying a lower maximum value than the preceding one. However, as time progresses, this pattern undergoes a reversal, leading to an eventual increase in the maximum values of these correlations. By increasing the parameter value of λ_1 to 15 in Fig. 2(c), it is evident that the quantum correlations undergo a noteworthy enhancement. Initially, at the onset of the scaled temporal evolution, quantum entanglement and steering exhibit an equivalence in their magnitudes, while the lower bounds of non-locality $\mathbb{B}_n$ are reduced. However, as time progresses, all three quantifiers exhibit a decreasing trend, which can be attributed to the influence of the decay rate $\gamma = 0.01$. Notably, non-locality experiences a more rapid decrease toward zero compared to steering and entanglement. Subsequently, upon further increasing λ_1 to 30, as depicted in Fig. 2(e), we observe a more pronounced enhancement in the three quantifiers and an increase in the number of oscillations. Notably, the entanglement curve $\mathscr{C}$ becomes distinct from the steering curve $\mathscr{S}_3$ as time advances, with steering converging to zero while entanglement tends toward a residual value.

In the context of the second scenario, where $\mu = 0$ (right panel), and keeping the conditions consistent with those presented in Figs. 2

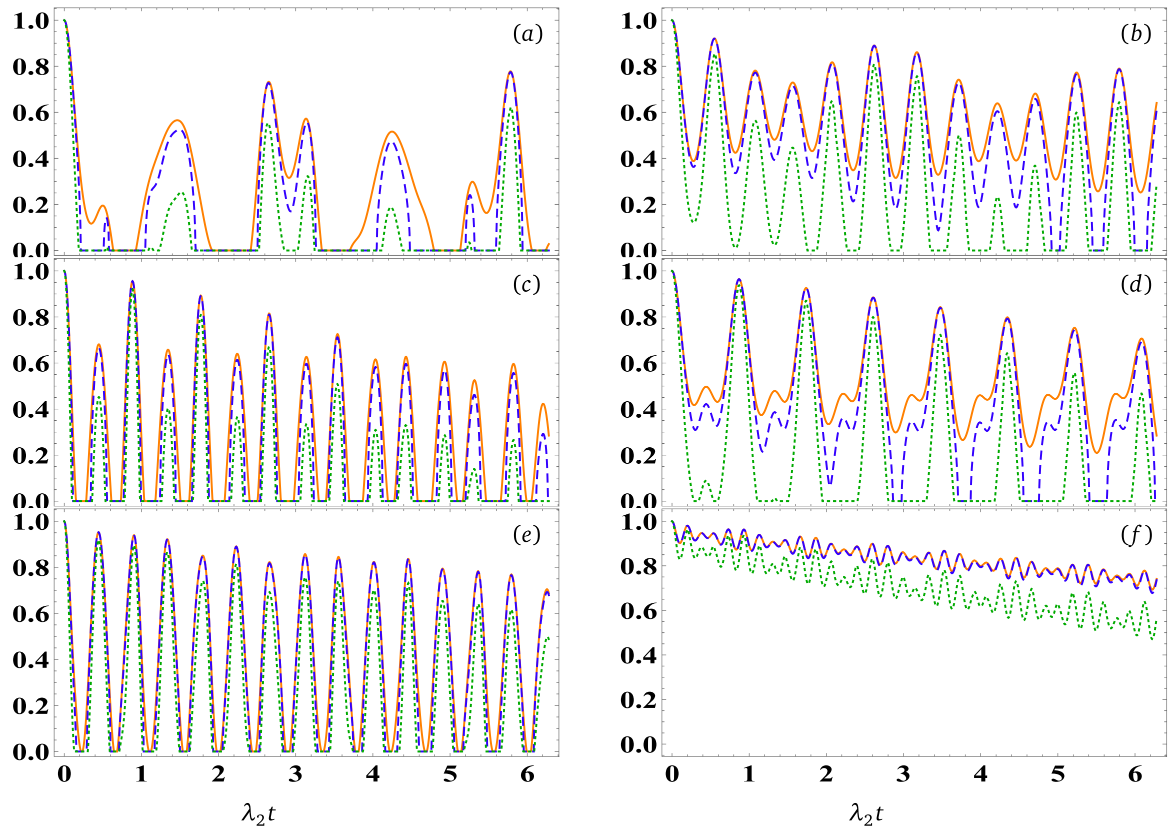

Fig. 3. The temporal evolution of quantum correlations $\mathscr{C}$ (solid-orange-curve), $\mathscr{S}_3$ (dashed-blue-curve), and $\mathbb{B}_n$ (dotted-green-curve) against the scaled time $\lambda_2 t$, where $\theta = \pi/2$, $n = 0$, and $\gamma = 0.01$. In the Left panels: $\mu = 1$, (a) $\Delta = 2$, $\lambda_1 = 10$ (b) $\Delta = 7$, $\lambda_1 = 10$. (c) $\Delta = 7$, $\lambda_1 = 30$. In the right panels: (b, d, f) are the same as (a, c, e), but $\mu = 0$.

(a, c, e), a distinct overall behavior is observed for the three quantifiers. At $\lambda_1 = 5$, these three functions exhibit corresponding oscillations at their maximum values. However, the presence of a decay rate diminishes the quantum correlations. Increasing λ_1 reveals a convergence of the maximum bounds for steering and entanglement, while their minimum bounds diverge. Non-locality exhibits similar oscillatory behavior, consistently remaining below the bounds observed for steering and entanglement. Upon further increasing λ_1 to 30, the steering and entanglement tend to exhibit greater similarity over time. A comparison of Figs. 2 (c, e) with Figs. 2 (d, f) reveals that in the first scenario (μ= 1), the three quantifiers reach zero more rapidly than in the second scenario (μ= 0). In the second scenario, steering and entanglement exhibit a stronger relationship with each other than in the first scenario. Consequently, it becomes evident that enhancing the dipole coupling strength, and thus the robustness of quantum correlations, at μ= 0 surpasses the scenario where μ= 1.

The impact of varying detuning parameter Δ and dipole coupling parameter λ_1 on the dynamics of the three quantum quantifiers of the two initial atomic scenarios is displayed in Fig. 3. We have set the initial field in the vacuum state n = 0, with $\gamma = 0.01$, and $\theta = \pi/4$. For the first scenario, characterized by $\mu = 1$ with $\Delta = 2$ and $\lambda_1 = 10$, Fig. 3(a) underscores how the detuning parameter influences the overall behavior of quantum correlations. It deformed the general behavior of quantum correlations, and non-locality is observed at specific intervals. However, under identical conditions but with $\mu = 0$, Fig. 3(b) reveals a chaotic behavior exhibited by the three quantifiers. Notably, the maximally entangled state of the teleported state transitions into a partially entangled state. Over time, the oscillations in steering and non-locality tend to converge to zero. With an elevation in the detuning parameter (Δ = 7), with $\mu = 1$ and $\lambda_1 = 10$, Fig. 3(c) provides insights into the behavior of quantum correlations. As Δ increases, we observe a corresponding augmentation in the number of oscillations. The entangled teleported state through our channel undergoes oscillations between a partially entangled state and a de-entangled state. Consequently, the dynamics of steering and non-locality mirror this oscillatory pattern. In the case of $\mu = 0$, while maintaining $\Delta = 7$, and $\lambda_1 = 10$, Fig. 3(d) demonstrates the input teleported entangled state, due to its interaction with the channel, turns into a partially entangled state over time. Notably, non-locality oscillates between zero and partial non-locality, while steering does not reach zero until a certain time has elapsed. Fig. 3(e) shows the dynamics of teleported quantum correlations with $\mu = 1$, influenced by the increase of the detuning parameter $\Delta = 7$ and dipole coupling $\lambda_1 = 30$. An enhancement is observed across the three quantifiers because of increasing λ_1, where there are increases in the maximum bounds, and reducing in periods of de-entanglement. This positive trend is enhanced in the case of $\mu = 0$, where the three quantifiers tend to a maximally correlated state. The presence of the decay factor in the dephasing environment induces an apparent decay in the system's overall behavior over time. However, the dipole coupling counteracts this detrimental effect by reorganizing the inherent randomness and decay arising from the detuning parameter. In essence, the dipole coupling plays a crucial role in enhancing quantum correlations, ultimately leading to an increase in the maximum bounds achievable.

Fig. 4 exhibits the influence of increasing the number of photons (n) on the teleported quantum correlations under varying dipole coupling (λ_1) conditions. When $\mu = 1$, $n = 1$, and $\lambda_1 = 5$, Fig. 4(a) illustrates that the number of oscillations amplifies with the growing photon count. Notably, entanglement and steering exhibit a nearly identical trend at their maximum values, while the minimum bounds of steering diminish more rapidly than those of entanglement. The minimum bounds of non-locality approach zero, while the maximum bounds exhibit a non-monotonic behavior, initially decreasing and then increasing again. Interestingly, under identical conditions but with $\mu = 0$ (as shown in Fig. 4(b)), entanglement persists over time, whereas both steering

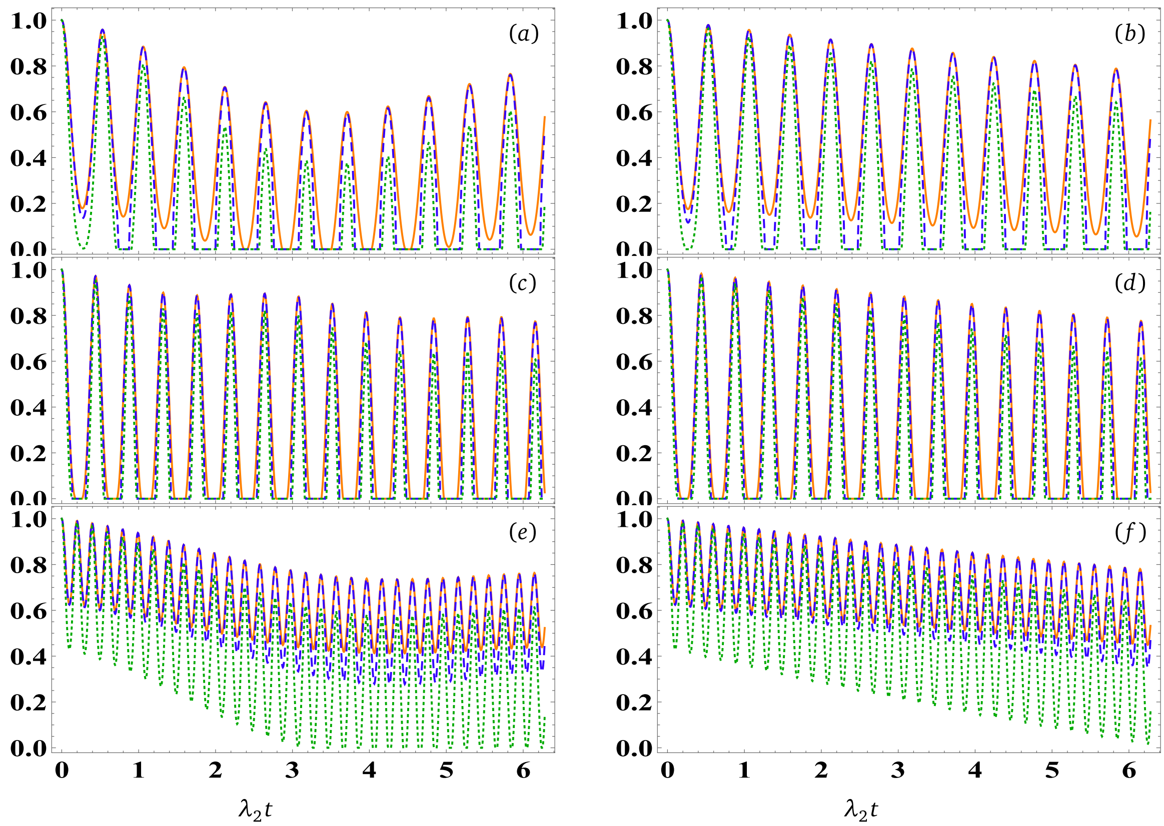

Fig. 4. The temporal evolution of quantum correlations $\mathscr{C}$ (solid-orange-curve), $\mathscr{S}_3$ (dashed-blue-curve), and $\mathbb{B}_n$ (dotted-green-curve) against the scaled time $\lambda_2 t$, where $\theta = \pi/2$, $\Delta = 0.1$, and $\gamma = 0.01$. In the Left panels: $\mu = 1$, (a) n=1, $\lambda_1 = 10$ (b) $n = 10$, $\lambda_1 = 5$. (c) $n = 5$, $\lambda_1 = 30$. In the right panels: (b, d, f) are the same as (a, c, e), but $\mu = 0$.

and non-locality vanish completely. Upon raising the photon count to $n = 5$, with $\lambda_1 = 5$, both scenarios, $\mu = 1$ and $\mu = 0$, displayed in Figs. 4(c) and (d), exhibit similar behaviors. They share nearly identical maximum bounds and a comparable number of oscillations. This suggests that the photon count plays a mitigating role in negating the influence of initial state parameters. Based on elevating the dipole coupling value to $\lambda_1 = 30$, while keeping $n = 5$, Figs. 4 (e), and (b) illustrate a notable augmentation in the number of oscillations and the amplification of maximum bounds. In this context, the minimum bounds exhibit enhancement but do not reach zero as readily. This decay over time can be attributed to the interaction with the dephasing environment.

Fig. 5 depicts the impact of the dephasing environment, characterized by $\gamma = 0.07$, on the three quantum quantifiers and how the coupling dipole contributes to the augmentation of maximum bounds in quantum correlations. Figs. 5(a) and (b) shed light on how the initial state can sustain quantum correlations. However, it is worth noting that when the initial states are maximally entangled, the three phenomena for $\mu = 0$ exhibit greater resilience to the effects of the dephasing environment compared to the case of $\mu = 1$, where the maximum bounds are notably higher at $\mu = 0$ (Figs. 5 (c) and (d)). It becomes evident that with an increase in the dipole coupling strength to $\lambda_1 = 30$, there is a clear enhancement in the maximum bounds of the three quantum measures, accompanied by an increase in the number of oscillations. Although non-locality and steering diminish over time, entanglement does not reach zero within the measured time-frame. The strength of entanglement depends on the initial state of the system. This highlights the crucial role played by the initial state of the channel in shaping the dynamics of instantaneously transmitted quantum correlations, while the dipole coupling enhances entanglement and mitigates the impact of the surrounding thermal environment on the teleported state's entanglement.

6. Conclusion

This paper has examined the teleportation process of a pair of entangled qubits traversing a channel composed of interacting atoms immersed in a quantum field, all within the confines of a dephasing environment. The primary focus of our investigation revolved around the comprehensive analysis of entanglement, steering, and non-locality exhibited by the teleported state, particularly concerning the channel parameters. The key factors under scrutiny encompassed the dipole coupling, detuning, photon number, and the influence exerted by the surrounding dephasing environment. Notably, our study has been grounded in the assumption that the channel atoms commence with a state of maximal entanglement, following two distinct scenarios, while the quantum field remains in a number state.

Our results showed that the initial state of the channel system has a clear effect on the state to be teleported and its associated quantum correlations. Furthermore, a noteworthy enhancement in quantum correlations has been observed with the escalation of dipole coupling. This amplification has been particularly evident in the transformation of the teleported state, transitioning from a de-entangled state to a partially entangled state. The minima of steering and non-locality have also experienced elevation in response to heightened coupling levels.

As we increased the detuning parameter, we observed the distortion of quantum correlations, accompanied by heightened oscillations. Notably, increasing the dipole coupling reconfigured these oscillations and mitigated the adverse effects resulting from detuning. Furthermore, the increase in the photon number amplified the oscillations, making the teleported state less reliant on the initial atomic state. Coupling this heightened photon count with the double coupling effect led to a marked enhancement in the maximum values of quantum correlations. Conversely, the interaction of our system with the dephasing environment diminished the strength of quantum correlations in the

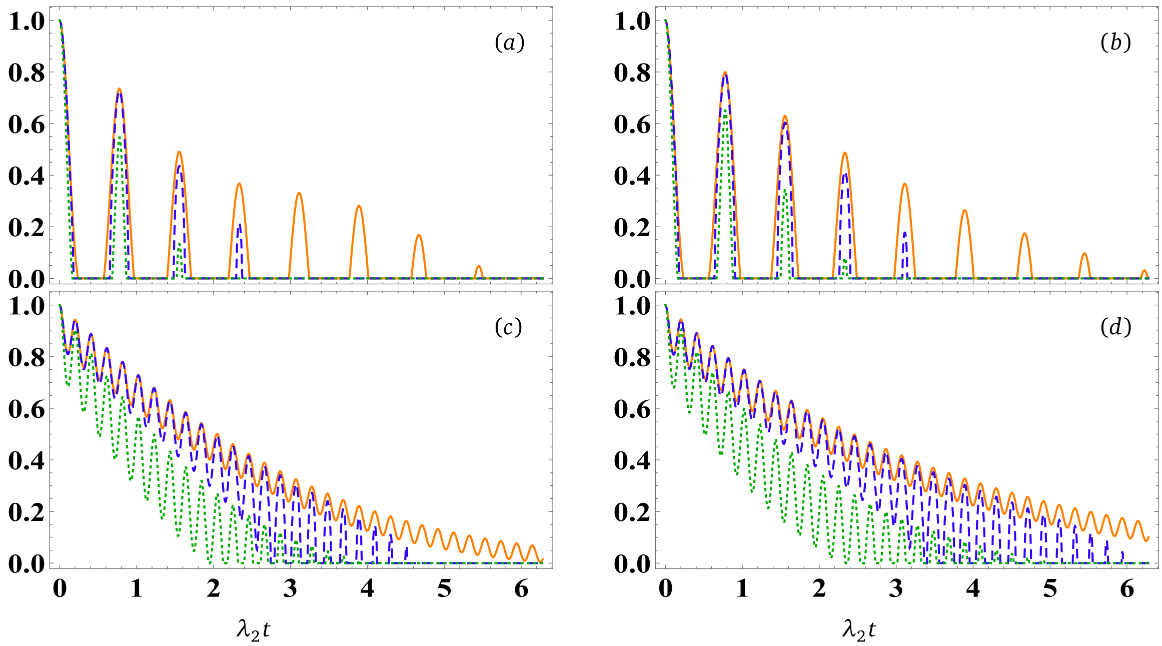

Fig. 5. The temporal evolution of quantum correlations $\mathscr{C}$ (solid-orange-curve), $\mathscr{S}_3$ (dashed-blue-curve), and $\mathbb{B}_n$ (dotted-green-curve) against the scaled time $\lambda_2 t$, where $\theta = \pi/2$, $\Delta = 0.1$, $n = 1$, and $\gamma = 0.07$. In the Left panels: $\mu = 1$, (a) $\lambda_1 = 5$ (b) $\lambda_1 = 30$. In the right panels: (b, d) are the same as (a, c), but $\mu = 0$.

teleported state. However, the dipole coupling played a significant role in mitigating this interaction's influence.

CRediT authorship contribution statement

Hanaa Abu-Zinadah: Writing – original draft, Methodology, Conceptualization. **E.M. Khalil:** Writing – review & editing, Writing – original draft, Software, Methodology, Investigation, Conceptualization.

Declaration of competing interest

The authors declare that they have no known competing financial interests or personal relationships that could have appeared to influence the work reported in this paper.

Acknowledgments

This work was funded by the University of Jeddah, Jeddah, Saudi Arabia under grant No. (UJ-23-DR-220). Therefore, the authors thanks the University of Jeddah for its technical and financial support.

References

Abd-Rabbou, M.Y., Ali, S.I., Metwally, N., 2023a. Detraction of decoherence that arises from the acceleration process. J. Opt. Soc. Am. B 40 (3), 585–593.

Abd-Rabbou, Mahmoud Youssef, Khalil, Eied Mahmoud, 2022. Dense coding and quantum memory assisted entropic uncertainty relations in a two-qubit state influenced by dipole and symmetric cross interactions. Ann. Phys. (Berl.) 534 (9), 2200204.

Abd-Rabbou, M.Y., Khalil, E.M., Al-Awfi, Saud, 2023b. Noise-based damping of chaotic entanglement in pulsed driven two-qubit system. Ann. Phys. (Berlin) 2300423.

Abd-Rabbou, M.Y., Khalil, E.M., Al-Awfi, Saud, 2024. Probing teleported quantum correlations in a two-qubit system inside a coherent field. Optik 296, 171551.

Abd-Rabbou, M.Y., Metwally, N, Ahmed, M.M.A., Obada, A.-S.F., 2019. Suppressing the information losses of accelerated qubit–qutrit system. Int. J. Quantum Inf. 17 (04), 1950032.

Abd-Rabbou, M.Y., Metwally, N., Ahmed, M.M.A., Obada, A.-S.F., 2022. Improving the bidirectional steerability between two accelerated partners via filtering process. Modern Phys. Lett. A 37 (22), 2250143.

Abd-Rabbou, M.Y., Shamirzaie, M., Khan, Salman, 2023c. Non-classical correlations of accelerated observers interacting with a classical stochastic noise beyond the single mode approximation. Opt. Quantum Elect. 55 (8), 715.

Abd-Rabboul, M.Y., Al-Barakaty, A., Abu-Zinadah, Hanaa, 2021. Quantum Fisher information of a teleported state in heisenberg XYZ chain with magnetic field and Kaplan–Shekhtman–Entin-Wohlman–Aharony interaction. IEEE Access 9, 51325–51331.

Almeida, Marcelo P, de Melo, Fernando, Hor-Meyll, Malena, Salles, Alejo, Walborn, S.P., Ribeiro, P.H. Souto, Davidovich, Luiz, 2007. Environment-induced sudden death of entanglement. Science 316 (5824), 579–582.

Asban, Shahaf, García de Abajo, F. Javier, 2021. Generation, characterization, and manipulation of quantum correlations in electron beams. npj Quantum Inf. 7 (1), 42.

Bellomo, B., Lo Franco, R., Compagno, G., 2008. Entanglement dynamics of two independent qubits in environments with and without memory. Phys. Rev. A 77, 032342.

Bouwmeester, Dirk, Ekert, Artur K., Zeilinger, Anton, 2013. The Physics of Quantum Information: Quantum Cryptography, Quantum Teleportation, Quantum Computation. Springer Science & Business Media.

Cao, Leiming, Du, Jinjian, Feng, Jingliang, Qin, Zhongzhong, Marino, Alberto M, Kolobov, Mikhail I, Jing, Jietai, 2017. Experimental observation of quantum correlations in four-wave mixing with a conical pump. Opt. Lett. 42 (7), 1201–1204.

Clauser, John F., Horne, Michael A., Shimony, Abner, Holt, Richard A., 1970. Proposed experiment to test local hidden variable theories. Phys. Rev. Lett. 24, 549.

Coffman, Valerie, Kundu, Joydip, Wootters, William K., 2000. Distributed entanglement. Phys. Rev. A 61, 052306.

Costa, A.C.S., Angelo, R.M., 2016. Quantification of Einstein-Podolsky-Rosen steering for two-qubit states. Phys. Rev. A 93, 020103.

Ding, Dong-Sheng, Zhou, Zhi-Yuan, Shi, Bao-Sen, Zou, Xu-Bo, Guo, Guang-Can, 2012. Generation of non-classical correlated photon pairs via a ladder-type atomic configuration: Theory and experiment. Opt. Express 20 (10), 11433–11444.

Fan, Xiao-Gang, Yang, Huan, Ming, Fei, Wang, Dong, Ye, Liu, 2021. Constraint relation between steerability and concurrence for two-qubit states. Ann. Phys. 533 (8), 2100098.

Fanchini, FF, Werlang, T, Brasil, CA, Arruda, LGE, Caldeira, AO, 2010. Non-Markovian dynamics of quantum discord. Phys. Rev. A 81 (5), 052107.

Gallego, M. Angeles, Coto, Raúl, Orszag, Miguel, 2012. Generation of quantum correlations for two qubits through a common reservoir. Phys. Scr. 2012 (T147), 014012.

Gisin, Nicolas, Thew, Rob, 2007. Quantum communication. Nat. Photon. 1 (3), 165–171.

Guo, You-Neng, Zeng, Ke, Chen, Ping-Xing, 2019. Teleportation of quantum Fisher information under decoherence channels with memory. Laser Phys. Lett. 16 (9), 095203.

Hiroshima, Tohya, 2001. Optimal dense coding with mixed state entanglement. J. Phys. A: Math. Gen. 34 (35), 6907.

Hu, Ming-Liang, 2012. Disentanglement, bell-nonlocality violation and teleportation capacity of the decaying tripartite states. Ann. Phys., NY 327 (9), 2332–2342.

Hu, Ming-Liang, Xi, Xiao-Qiang, Lian, Han-Li, 2009. Thermal and phase decoherence effects on entanglement dynamics of the quantum spin systems. Physica B: Cond. Matt. 404 (20), 3499–3506.

Khalil, E.M., Abd-Rabbou, M.Y., 2022. Robustness of a teleported state influenced by dipole interaction and magnetic field under intrinsic decoherence. Optik 267, 169703.

Krzywda, Jan, Roszak, Katarzyna, 2016. Phonon-mediated generation of quantum correlations between quantum dot qubits. Sci. Rep. 6 (1), 23753.

Ladd, Thaddeus D, Jelezko, Fedor, Laflamme, Raymond, Nakamura, Yasunobu, Monroe, Christopher, O'Brien, Jeremy Lloyd, 2010. Quantum computers. Nature 464 (7285), 45–53.

Lee, Jinhyoung, Kim, M.S., 2000. Entanglement teleportation via werner states. Phys. Rev. Lett. 84, 4236–4239.

Man, Zhong-Xiao, Xia, Yun-Jie, Franco, Rosario Lo, 2018. Temperature effects on quantum non-Markovianity via collision models. Phys. Rev. A 97 (6), 062104.

Manzano, Daniel, 2020. A short introduction to the Lindblad master equation. Aip Adv. 10 (2).

Mirmasoudi, F., Ahadpour, S., 2018. Dynamics of super quantum discord and optimal dense coding in quantum channels. J. Phys. A 51 (34), 345302.

Mohammed, Nagwa Ibrahim, Abdelsalam, Hanadi M, Almalki, Shaimaa, Abd-Rabbou, M.Y., Abdel-Khalek, S., Khalil, E.M., 2023. Witnessing quantum correlations in two coupled quantum dots under intrinsic decoherence. Alex. Eng. J. 69, 521–527.

Omri, Mohamed, Abd-Rabbou, M.Y., Khalil, E.M., Abdel-Khalek, S, 2022. Thermal information and teleportation in two-qutrit Heisenberg XX chain model. Alex. Eng. J. 61 (10), 8335–8342.

Rahman, Atta ur, Abd-Rabbou, M.Y., Haddadi, Saeed, Ali, Hazrat, 2023. Two-qubit steerability, nonlocality, and average steered coherence under classical dephasing channels. Ann. Phys. (Berl.) 535 (4), 2200523.

Wang, Z.S., 2009. Geometric quantum computation and dynamical invariant operators. Phys. Rev. A 79 (2), 024304.

Yan, Xue Qun, Yue, Zhuan Lin, 2013. Dynamics of quantum and classical correlations of a two-atom system in thermal reservoirs. Chaos Solit. Fractals 57, 117–122.

Youssef, M., Ali, S.I., Abd-Rabbou, M.Y., Obada, A.-S.F., 2023. Exploring quantum correlations of two-qubit heisenberg chain model influenced by magnetic dipole–dipole, magnetic field, and a symmetric cross interaction. Quantum Inf. Process. 22 (6), 229.

Yu, Ting, Eberly, J.H., 2009. Sudden death of entanglement. Science 323 (5914), 598–601.